Journal of Porous Materials (2021) 28:751–762
https://doi.org/10.1007/s10934-020-01030-8

Synthesis of gold nanoparticles immobilized on fibrous nano-silica for latent fingerprints detection

Shuoyun Wei[1] · **Xiaohu Cui**[1]

Accepted: 26 December 2020 / Published online: 25 January 2021

Abstract
Fingerprint, as the main basis of individual identification, plays a vital role in various areas, including criminal investigation and forensic detection. Accordingly, it is highly significant to develop methods for fingerprint detection with high sensitivity and accuracy. In this study, Au@KCC-1 nanocomposites with easy accessibility of active sites were prepared by a convenient method, and the feasibility of obtained Au@KCC-1 nanocomposites were finally investigated on latent fingerprints detection. Due to the immobilization effect of the KCC-1 carrier on Au NPs, the formed Au@KCC-1 nanocomposites showed stable chemical structures, excellent selectivity, and high sensitivity. Using Au@KCC-1 nanocomposites as a new type of fingerprint powders, latent fingerprints could be enhanced with clear patterns, satisfactory ridge details, and even sweat pores, and it was successfully employed to enhance latent fingerprints deposited on various object surfaces (such as blue plastic, black paper, foundation box, red cardboard, glass, and plastic Blue-ray CD discs (the smooth side)) for individual identification. The results demonstrated that Au@KCC-1 nanocomposites powders could be an alternative to commercially available fingerprint powdering reagents in forensic detection in the future.

Keywords Fibrous nano-silica · Gold nanoparticles · Au@KCC-1 nanocomposites · Latent fingerprints · Forensic science

1 Introduction

Fingerprint refers to the contact pattern left on the surface of an object when the finger touches this object, which can reflect the morphological characters of the fingerprint. With the characteristics of the uniqueness, immutability, and complexity of fingerprints, fingerprint identification has become one of the most essential personal identification methods in the fields of criminal investigation, access control, and law enforcement [1–6]. With the rapid development of science and technology and the increasing awareness of criminal suspects on anti-investigation, most fingerprints left at the crime scenes are latent, and it is challenging to identify latent fingerprints with the naked eye. Therefore, a variety of optical contrast agents have been developed in the past decades to identify latent fingerprints, such as powders dusting, cyanoacrylate fuming, silver nitrate, ninhydrin, 1,8-Diazafluoren-9-one approach, and small particle reagent approach [7]. However, these traditional visualization methods suffer from low contrast, low sensitivity and selectivity, high toxicity (impact on human health and DNA damage), the high limit of detection, and so on. To overcome these problems, fluorescent nanocomposites are gaining popularity [8–12]. But recent synthesized fluorescent nanocomposites (such as quantum dots, fluorescent carbon dots, rare earth up-conversion materials, metal nanoclusters, etc.) still suffer complex preparation process, low detection efficiency, and photobleaching problems [13–17]. So far, gold nanoparticles have attracted immense attention in forensic sciences due to their excellent physicochemical properties and good biocompatibility. Since 1989, gold nanomaterials [18] have been firstly applied to latent fingermark development in the multi-metal deposition (MMD) method. On the basis of MMD technique, Stauffer et al. [19] have presented the single-metal deposition (SMD) for the development of latent fingermarks by a gold enhancement procedure. It has been discovered that gold nanoparticles could not only adhere

The authors contributed to the work equally and should be regarded as co-first authors.

✉ Shuoyun Wei
weisy@163.com

[1] Key Laboratory of Evidence Science Techniques Research and Application of Gansu Province, College of Public Security Technology, Gansu University of Political Science and Law, Lanzhou 730070, People's Republic of China

easily to the latent fingerprint ridges rather than furrows [20], but also preserve developed fingerprints for a long term due to their inert nature [21]. At present, the technologies of metal deposition and small particle reagent are the most commonly reported in the literature, but some of gold nanomaterials require the use of complicated reactants, strict pH range, extensive time, and bothersome preparation processes [11]. Hence, there is an urgent need to develop a new kind of gold nanomaterials for latent fingerprints detection.

In recent years, various nanocomposites containing amorphous silica have been proposed [22–26]. As a carrier material, silica provides physicochemical stability, biocompatibility, and an easily functionalized surface. Besides, it is reported that silica-based nanoparticles exhibit lower detection limits towards fingerprints by surface modification [27]. Huang et al. have used organic ligands to modify silica nanocomposites to develop latent fingerprints [28]. However, some of these reported nanoparticles still have large diameter, limiting the detection of the third level features of latent fingerprints. Moreover, the in-situ doping approach during the synthesis of nanocomposites also inevitably affects the morphology and structure of silica-based nanoparticles [29]. Therefore, it remains a challenge to improve the interaction between silica-based nanoparticles and latent fingerprints by choosing suitable organic molecules for surface modification [27].

Recently, Polshettiwar et al. [30] have reported well-defined porous silica nanospheres with fibrous pore morphology, so-called dendritic mesoporous silica nanospheres (MSNs) (named KCC-1). Because of its special fibrous morphology, KCC-1 has a larger surface area than conventional MSNs (like SBA-15 or MCM-41) [31–34]. Dong et al. [35] have investigated the immobilization of silver nanoparticles on amino-functionalized KCC-1 which exhibited excellent catalytic activity for the reduction of 4-nitrophenol and 2-nitroaniline in water at room temperature. Up to date, there is no report on KCC-1 supported Au NPs for latent fingerprints detection. Intrigued by this study, a high-performance nanomaterial was synthesized to make up for the deficiencies of currently available materials and then to be used for latent fingerprints detection for future case investigation.

This paper described the in-situ synthesis of Au NPs using KCC-1 as the carrier and investigated the application on latent fingerprints detection (Scheme 1). The in-situ growth way enhanced the combination strength of Au NPs and KCC-1-NH_2, so the as-prepared Au@KCC-1 nanocomposites presented excellent stability and sensitivity. Moreover, the Au@KCC-1 nanocomposites could be applied to detect latent fingerprints deposited on various objects, which were expected to be "green" nanocomposites for further application (such as touch DNA) due to the low toxicity and good biocompatibility of the Au@KCC-1 nanocomposites.

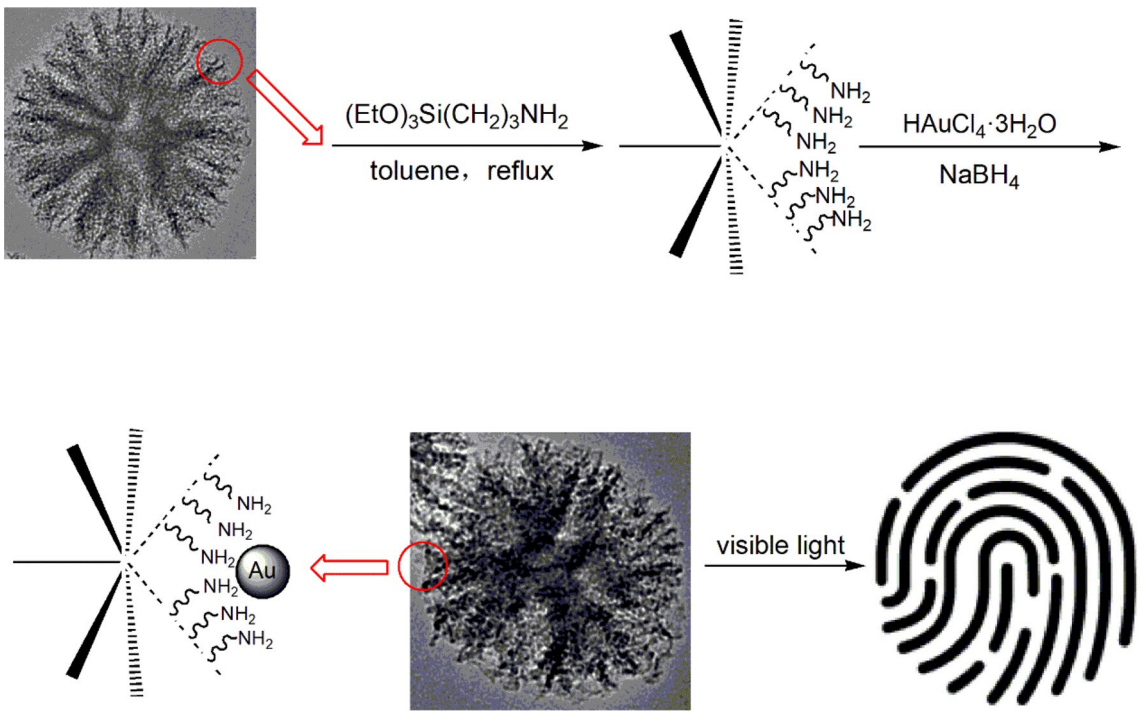

Scheme 1 Synthesis of Au@KCC-1 nanocomposites

2 Experimental

2.1 Chemicals

Urea (CH_4N_2O), hexadecylpyridinium bromide Hydrate ($C_{21}H_{38}BrN{\cdot}xH_2O$), tetraethyl orthosilicate ($C_8H_2OO_4Si$), cyclohexane (C_6H_{12}), pentanol ($C_5H_{12}O$), acetone (CH_3COCH_3), hydrogen tetrachloroaurate (III) trihydrate ($HAuCl_4{\cdot}3H_2O$), sodium borohydride ($NaBH_4$), 3-Aminopropyltriethoxysilane (3-APTES), and toluene were obtained from Shanghai Macklin Biochemical Co, Ltd (China). All reagents were used without further purification in experiments. Ultrapure water was used to prepare all the solutions in experiments.

2.2 Preparation of Au@KCC-1 nanocomposites

2.2.1 Preparation of fibrous nano-silica (KCC-1)

According to the previous report [35], KCC-1 was obtained by a hydrothermal method. TEOS (5 g) was dissolved in a solution of cyclohexane (60 mL) and 1-pentanol (3 mL). A stirred solution of cetyl pyridinium bromide (CPB 2 g) and urea (1.2 g) in water (60 mL) was then added. The mixture was continually stirred for a further 30 min at room temperature and then placed in a flask to heat at 90 °C for 10 h. The crude product was filtrated and washed with deionized water and acetone to obtain a pure product. This material was then calcined at 550 °C for 6 h in air.

2.2.2 Preparation of the aminopropyl-functionalized KCC-1

To synthesize KCC-1-NH_2, KCC-1 (0.2 g) and 3-APTES (0.36 g) were mixed in toluene (100 mL) and refluxed for 12 h under the nitrogen atmosphere. The white solid of aminopropyl-functionalized KCC-1 (KCC-1-NH_2) was finally obtained by filtration and washed successively with ethanol.

2.2.3 Preparation of Au@KCC-1 nanocomposites

Au@KCC-1 nanocomposites were obtained by a liquid-phase reduction method. KCC-1-NH_2 (0.2 g) was ultrasonically dispersed in H_2O (100 mL), before the addition of $HAuCl_4{\cdot}3H_2O$ (0.0099 g, 3 mL). After being stirred for about 3 h, an excess $NaBH_4$ solution was slowly dropped. The Au nanoparticles (Au NPs) were formed and anchored on the aminopropyl-functionalized fibrous silica when the above-mixed solutions were reacted for 3 h. Finally, the Au@KCC-1 nanocomposites were obtained by filtration and dried in a vacuum.

2.3 Characterization

The microstructures of the Au@KCC-1 nanocomposites were characterized by a JSM-5600LV scanning electron microscope (Electro-Optics Corporation, Japan). The morphology and microstructure of the Au@KCC-1 nanocomposites were observed by Tecnai G^2F^{30} transmission electron microscopy, and samples were obtained by placing a drop of a colloidal solution onto a copper grid and evaporating the solvent in the air at room temperature. The absorption spectra of the Au@KCC-1 nanocomposites was measured with a lambda 950 UV–visible absorption spectrophotometer (PerkinElmer Corporation, US). Fourier transform infrared spectra were performed on a Nicolet NEXUS 670 FTIR spectrometer with a DTGS detector, and samples were measured with KBr pellets. All spectra were obtained at 25 °C. X-ray powders diffraction were performed on Rigaku D/max-2400 diffractometer using Cu-Ka radiation as the X-ray source in the 2θ range of 10°–80°. XPS was conducted on the Kratos AXIS Ultra DLD photoelectron spectrometer (Kratos, UK) and the C1s line at 284.8 eV was used as the binding energy (BE) reference. Elemental analysis (Gmbh Vario El Elementar) and inductively coupled plasma (ICP, IRIS Advantage analyzer) were employed to measure the N, C, H, and Au content of the samples. A VSC6000 document imaging workstation (Foster & Freeman Ltd., UK) was employed to observe the treated fingerprints and take pictures. The particle size distribution of KCC-1 and the zeta potential of the Au@KCC-1 nanocomposites powders were measured by dynamic light scattering. (DLS, Malvern Zetasizer Nano ZS90, UK).

2.4 Detection of latent fingerprints

All latent fingerprint samples were obtained from a single volunteer. The volunteer's hands were washed several times with soap and then dried in air. The volunteer then pressed the latent fingerprints on the surface of substrates with even pressure after rubbing the fingertip across the forehead. Porous substrates (black papers, red cardboard) and smooth substrates (blue plastic, foundation box, glass, and plastic Blue-ray CD discs (the smooth side)) were employed for depositing latent fingerprints. Commercial gold powders and silver powders were selected as the control group.

3 Results and discussion

3.1 Synthesis and characterization of Au@KCC-1 nanocomposites

As illustrated in Scheme 1, the in-situ synthesis of Au@KCC-1 nanocomposites consisted of three steps. KCC-1, which was employed as the substrate, was obtained by the hydrothermal method. The aminopropyl functionalization of the KCC-1 surface was then conducted by covalent attachment of 3-APTES to obtain KCC-1-NH_2. The result showed that the content of C, N, H loaded on the surface of KCC-1 increased, indicating the successful synthesis of KCC-1-NH_2 (Table 1). Finally, KCC-1-NH_2 was treated with $HAuCl_4 \cdot 3H_2O$, followed by the reduction of $NaBH_4$. Though KCC-1 displayed a fibrous pore morphology structure, nearly no Au could be immobilized on the KCC-1 surface without aminopropyl functionalization, which may be attributed to the weak binding between KCC-1 and Au, and Au can be lost easily in the washing step. Since these aminopropyl groups were successfully grafted on the surface of KCC-1, they are well-spaced from each other. Thus, Au NPs could disperse uniformly on the surface of KCC-1.

Table 1 The content of C, N, H of KCC-1 and KCC-1-NH_2

Name	N	C	H
KCC-1	0.00	1.16	0.291
KCC-1-NH_2	3.14	10.38	2.082

To investigate the formation of fibrous morphology, FESEM and TEM measurements were first taken on fibrous silica KCC-1 and Au@KCC-1 nanocomposites. The FESEM image of bare KCC-1 carrier (Fig. 1a) showed relatively uniform-sized microspheres with clear bicontinuous concentric lamellar morphology [36, 37]. Besides, a three-dimensional spherical structure constituted by the dendrimeric fibers of KCC-1 was observed in Fig. 1b. Compared with KCC-1, nano-sized Au NPs were challenging to be detected by SEM (Fig. 1c). Hence, the elemental information of Au was investigated with the EDX spectrum (Fig. 1d). Moreover, ICP analysis results revealed that the content of Au loaded on the surface of

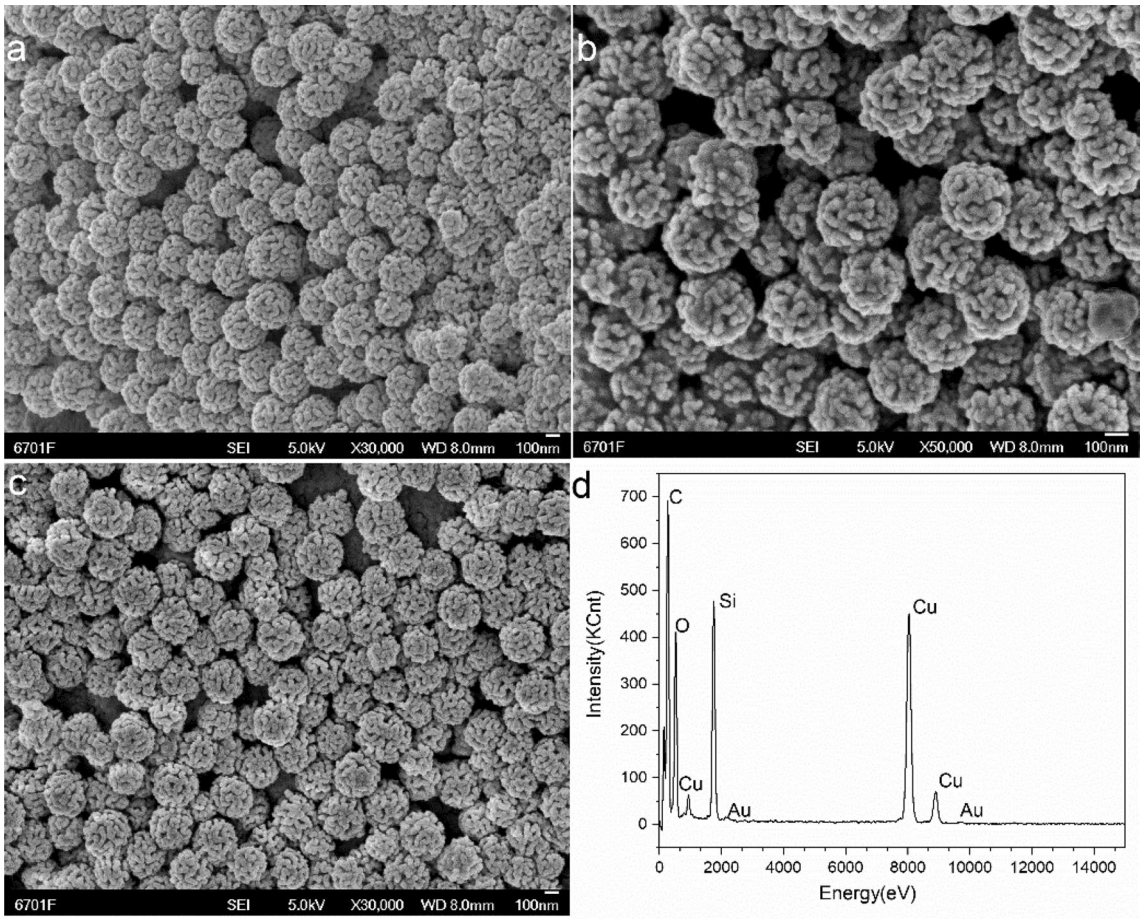

Fig. 1 **a** and **b** SEM images of KCC-1, **c** SEM image Au@KCC-1 nanocomposites, **d** EDX spectrum of Au@KCC-1 nanocomposites

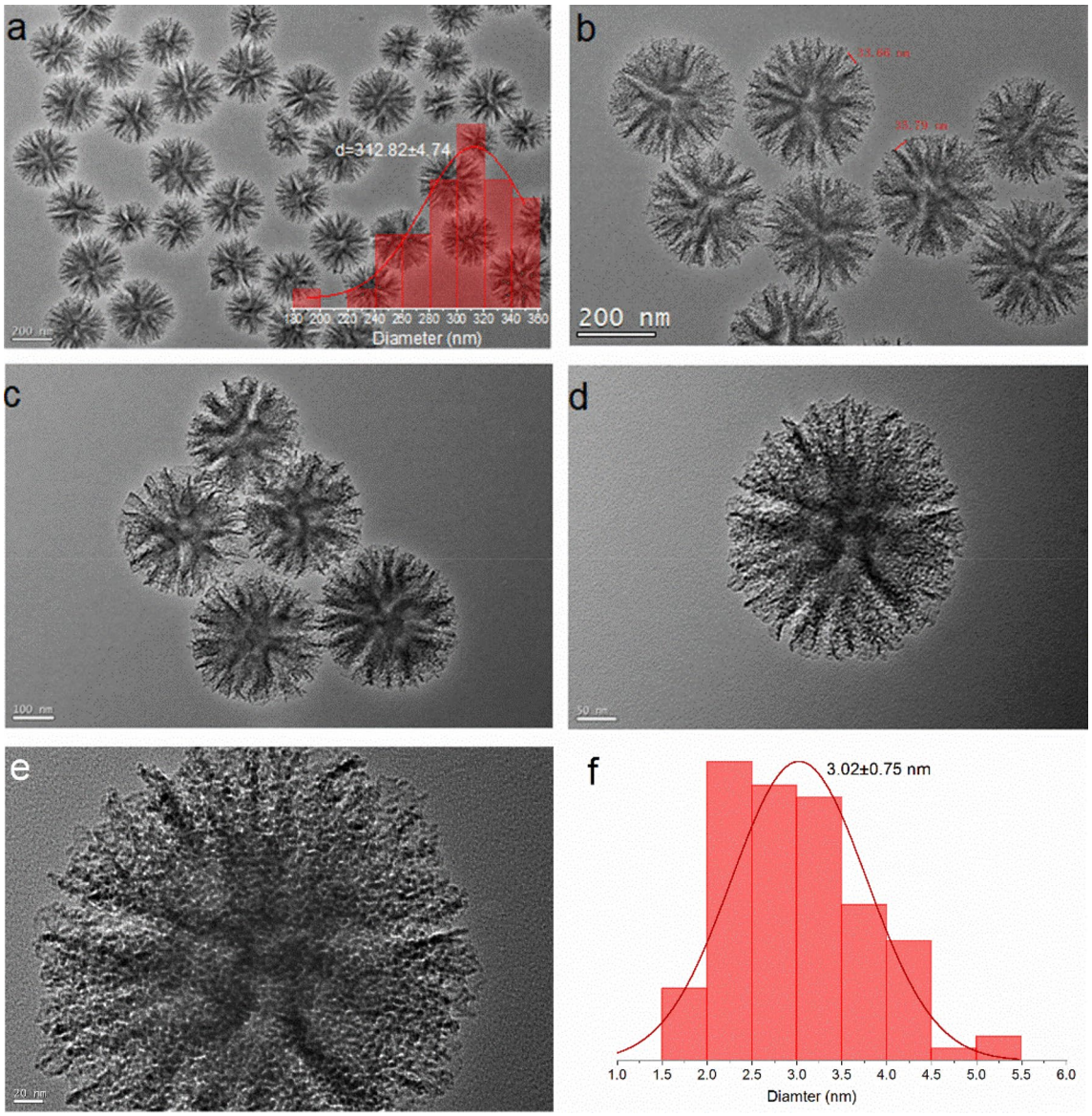

Fig. 2 **a** and **b** TEM images of KCC-1, **c**, **d** and **e** TEM images Au@KCC-1 nanocomposites, **f** The particle size distribution of Au@KCC-1 nanocomposites

KCC-1 was 1.66 wt%, indicating that Au NPs were successfully immobilized on fibrous nano-silica. From TEM images of KCC-1 (Fig. 2a and b), it can be found that the well-ordered fibers grew from the center of the microsphere and spread evenly in all directions to form fibrous spherical silica particles [38]. Therefore, KCC-1 had high accessibility, and this character could be useful for the formation of the silica-supported nanocomposites. As shown in Fig. 2a, the particle size distribution of KCC-1 microspheres with fibrous structure was about 312.82 ± 4.74 nm which was further confirmed by DLS analysis (314.2 nm). Figure 2b clarifies that these fibers were well dispersed with an approximately 33.66 nm distance from each other. This considerable distance between fibers and the high surface area of KCC-1 made it easy for Au NPs (diameters were 3.02 ± 0.75 nm) to load onto KCC-1. Besides, it is reported that KCC-1-NH_2 could help to avoid the aggregation of Au NPs and thus improved the accessibility of the active sites of Au@KCC-1 nanocomposites [35]. The TEM images of Au@KCC-1 nanocomposites were shown in Fig. 2c and d. As expected, Au NPs were evenly fixed between fibers of KCC-1 without leaching, and no evident aggregation was found, which could be attributed to the strong anchors effect of KCC-1-NH_2 [39]. The average size of Au NPs was 3.02 ± 0.75 nm (calculated from more than 200 Au NPs) (Fig. 2f).

The structure of the Au@KCC-1 nanocomposites was then analyzed with UV–vis spectra and FTIR spectra. Previous study has reported that Au NPs exhibited intense light scattering and absorption at around 520 nm because of localized surface plasmon resonance (LSPR) excited by the interaction between Au NPs and incident electromagnetic fields (lights) [40]. However, the position and the intensity of the absorption band of Au NPs can be affected by the size, shape, and Au loading [32, 41, 42]. As shown in Fig. 3a, Au@KCC-1 nanocomposites displayed maximum absorption at 530 nm in the UV–vis spectrum. This red-shift phenomenon of the LSPR band suggested that the diameters of formed Au NPs were larger than 2 nm [41, 43]. Figure 3b depicted the structure of KCC-1 (top one) and Au@KCC-1 nanocomposites (bottom one) by FTIR spectra. The bands at 966 and 1639 cm^{-1} were attributed to the Si–OH stretching and water molecules absorbed on the KCC-1 surface, respectively [44, 45], while the typical bands at around 1090 and 808 cm^{-1} were associated with the formation of a condensed silica network. The peak at wavenumber 2850–3000 cm^{-1} owed to the C–H stretching frequency of the 3-APTES molecules on the KCC-1 surface [35, 43, 46]. By comparing these two FTIR spectra, distinct intensities changes could be found in Au@KCC-1 nanocomposites (Fig. 3c), indicating the successful insertion of Au NPs into KCC-1.

The phase structures of KCC-1 and Au@KCC-1 nanocomposites were characterized by XRD measurements ranging from 10° to 80°. KCC-1 and Au@KCC-1 nanocomposites presented a broad signal at $2\theta = 22.15$ in Fig. 4a, which could be ascribed to the existence of amorphous silica [32]. However, no reflections from Au were observed in XRD spectra because the concentration of Au was low, and they were dispersed into very small particles [32, 47]. This phenomenon was consistent with the results of TEM analysis.

Finally, the chemical state and the elemental composition of the Au@KCC-1 nanocomposites were studied with XPS. A full-scan XPS spectrum for the as-prepared Au@KCC-1 nanocomposites was illustrated in Fig. 4b. Major peaks corresponding to Si, O, C, N, and Au can be clearly observed, and the presence of N1s (400.02 eV) further confirmed that KCC-1 had been successfully functionalized by 3-APTES. This result was consistent with the result of ICP and elemental analysis. As shown in Fig. 4c, the Au4f core level was fitted using one doublet (Au $4f_{7/2}$–Au$4f_{5/2}$) with a fixed area ratio equal to 4:3 and doublet separation at 3.65 eV. The high-resolution XPS Au 4f spectrum displays a doublet indicative of metallic Au, with binding energies of 83.95 and 87.6 eV for the Au$4f_{7/2}$ and Au$4f_{5/2}$ levels, demonstrating that most of the Au^{3+} ions were reduced successfully by $NaBH_4$. This was consistent with the literature values for supported Au NPs [32, 44].

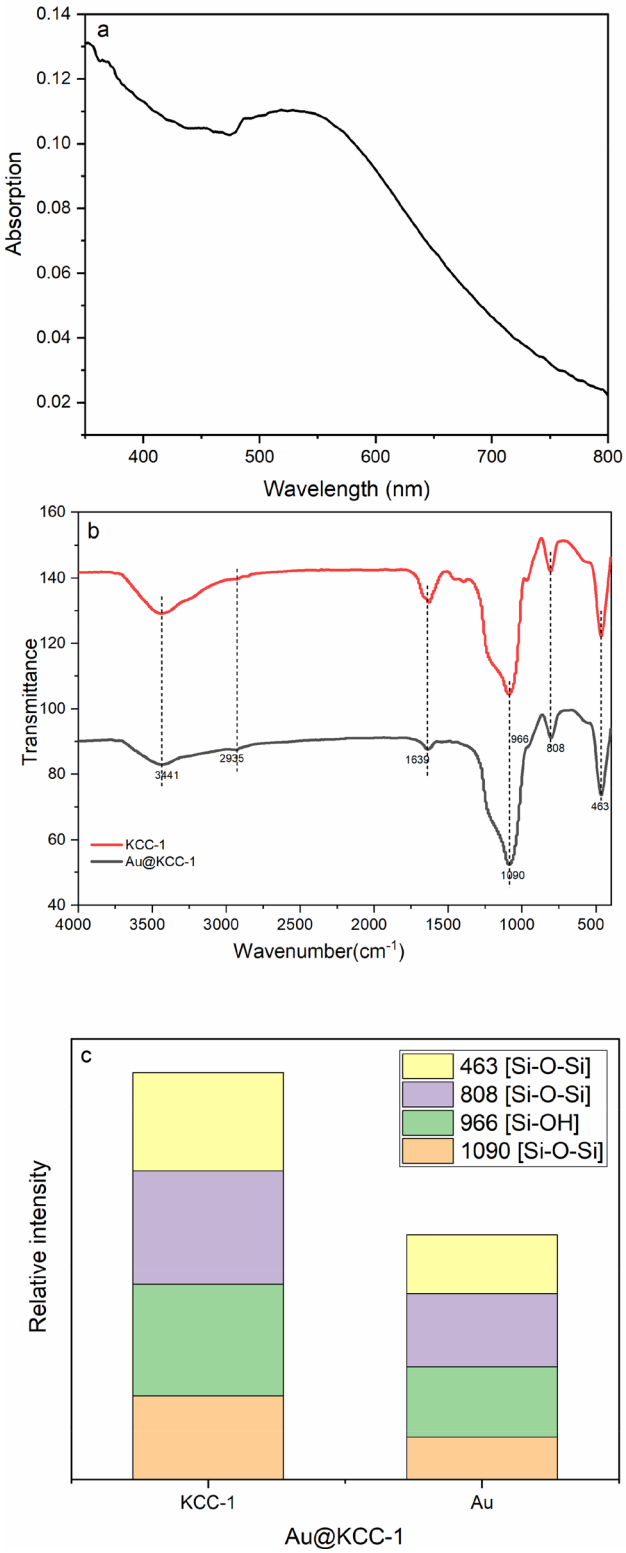

Fig. 3 **a** UV–visible absorption spectra of Au@KCC-1 nanocomposites, **b** FTIR spectra of KCC-1 and Au@KCC-1 nanocomposites, **c** The band intensities of Au@KCC-1 nanocomposites

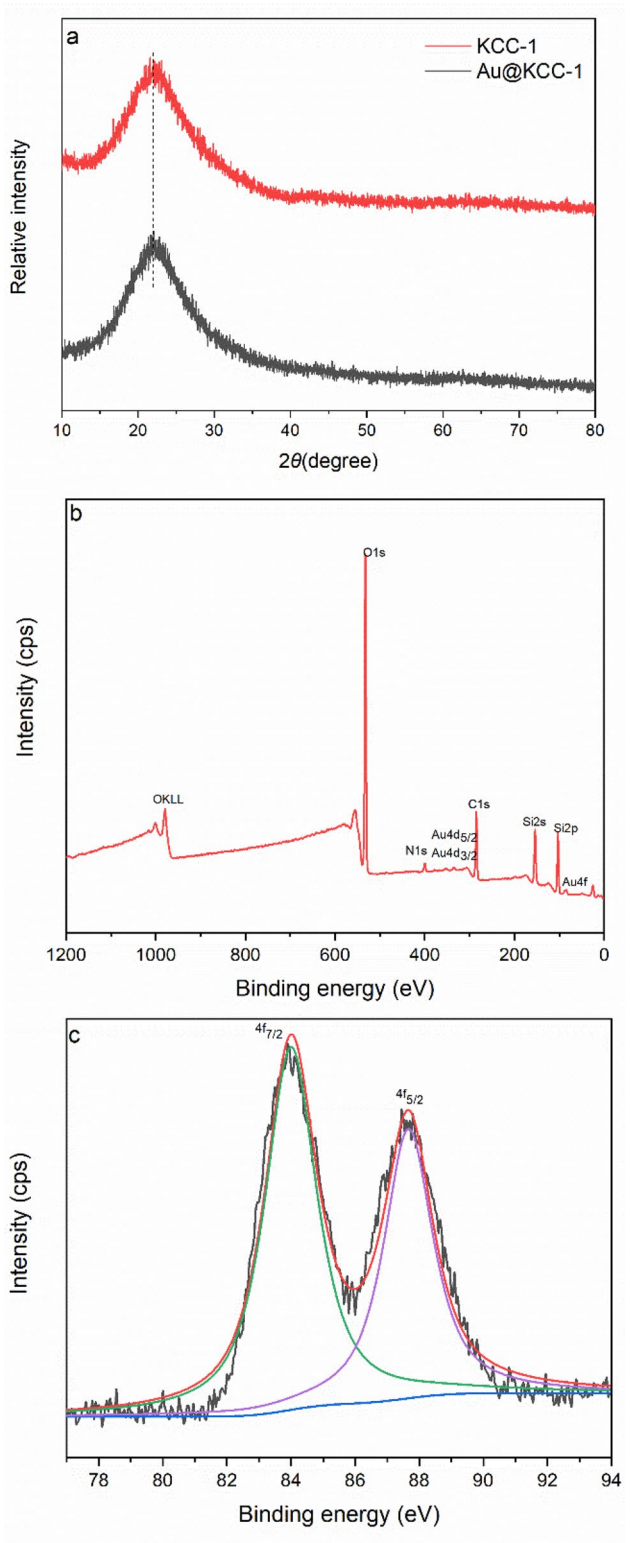

Fig. 4 **a** XRD pattern of KCC-1 and Au@KCC-1 nanocomposites, **b** XPS survey spectra of Au@KCC-1 nanocomposites, **c** XPS spectra of Au 4f

3.2 Application to latent fingerprints detection

Latent fingerprint residues normally contain natural secretions such as moisture from exocrine sweat glands and oily components from sebaceous glands [48, 49]. Therefore, powders dusting, relying on adsorption and electrostatic interactions between fingerprint powders and the moistures and oil constituents, is a commonly used physical method [50–52]. In this study, Au@KCC-1 nanocomposites were synthesized and selected as a new kind of powders for latent fingerprints detection because of their excellent properties like facile preparation, low cost, relatively chemical stability, good affinity with finger residues. It is known that the fingerprint residues contained natural secretions are the negatively charged [53, 54]. According to the DLS analysis, the zeta potential of Au@KCC-1 nanocomposites powders was 25.54 mV. Thus, the result of zeta potential analysis suggested that there were electrostatic interactions between the Au@KCC-1 nanocomposites and fingerprint residues.

Au@KCC-1 nanocomposites powders were applied in detecting latent fingerprints on common substrates in daily life, such as blue plastic, black paper, foundation box, red cardboard, glass, and plastic Blue-ray CD discs (the smooth side) to confirm the wide applicability and high contrast of Au@KCC-1 nanocomposites powders (Fig. 5a–f). Due to the good monodispersity and small particle sizes, Au@KCC-1 nanocomposites powders could be selectively attached to the papillary ridges of the fingerprint through electrostatic interactions with the residues (amino acids and proteins, etc.) rather than furrows. As shown in Fig. 5a′–f′, legible and clean-cut fingerprint images were observed on the above-mentioned substrates under the irradiation of visible light with high contrast and low background interferences. The high contrast and wide applicability of Au@KCC-1 nanocomposites powders should be attributed to the nano size, large specific surface area, and suitable affinity. These results indicated that the synthesized Au@KCC-1 nanocomposites powders could effectively enhance the latent fingerprints on the surface of different substrates.

To further discuss the contrast of fingerprint on different substrates, the grayscale value (G) was extracted from up to down along the selected red line areas in each picture using software Image J (Fig. 6a and c). The grayscale distribution was shown in Fig. 6b and d, and the grayscale value of eight consecutive groups of papillary ridges and furrows were listed in Table 2. The gray difference (D-value), which could reflect the contrast between papillary ridges and furrows, was calculated by averaging the difference between each group's grayscale values. For example, as shown in Table 2, the D-value of glass was higher than that of the foundation box. Therefore, the contrast of glass was higher than that of foundation box.

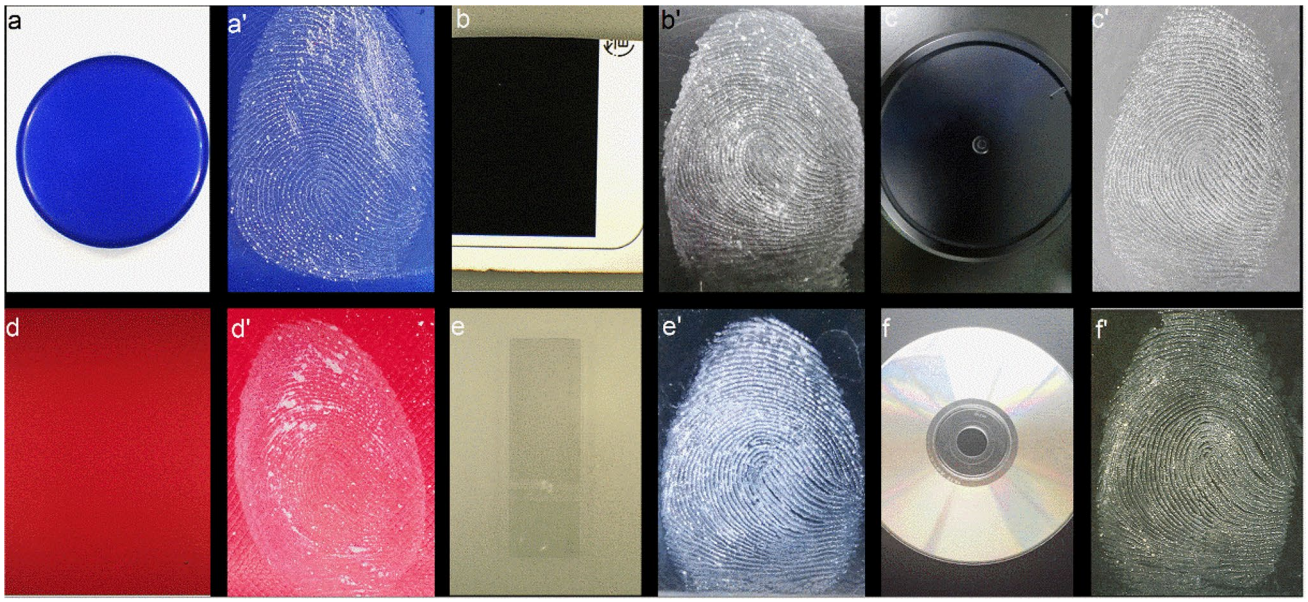

Fig. 5 Latent fingerprints on the surfaces of different substrates developed with the as-prepared Au@KCC-1 nanocomposites powders (**a**–**f**). **a**,**a′** plastic (blue); **b**,**b′** black paper; **c**,**c′** foundation box; **d**,**d′** cardboard (red); **e**,**e′** glass; **f**,**f′** plastic Blue-ray CD discs (the smooth side for burning). Images were taken under visible light, and a VSC6000 document imaging workstation was used to take pictures

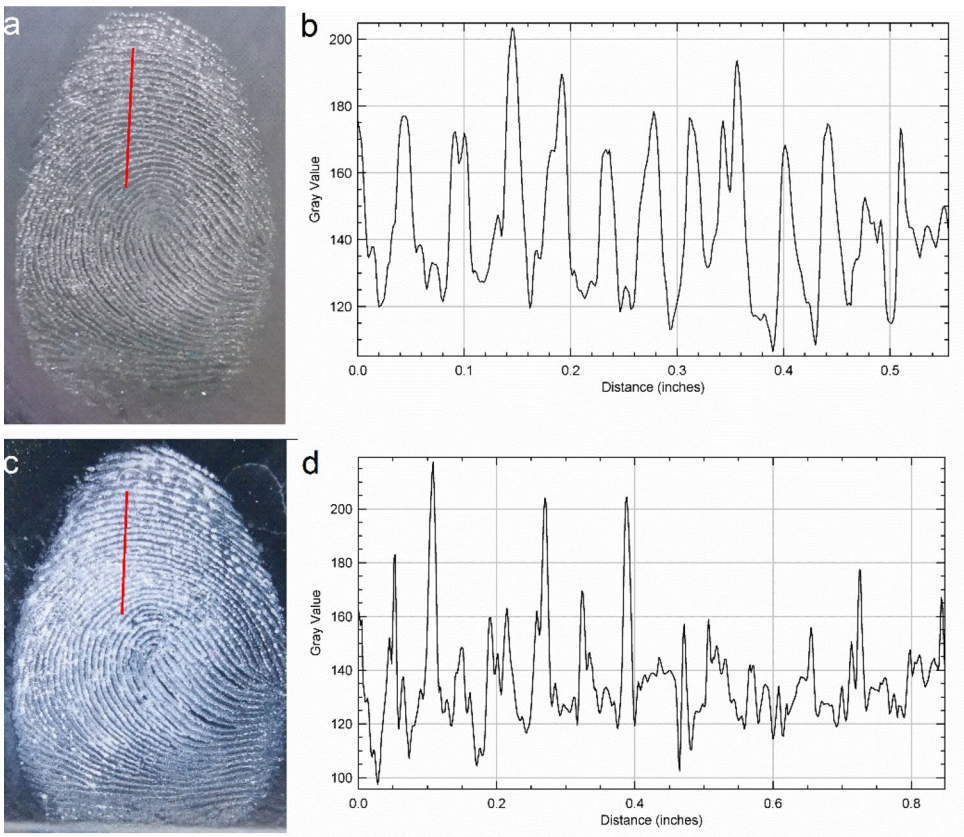

Fig. 6 Latent fingerprints on foundation box and glass developed with as-prepared Au@KCC-1 nanocomposites powders: **a** and **c** fingerprint images; **b** and **d** grayscale distribution diagram under the red line in each image

Sensitivity and selectivity of Au@KCC-1 nanocomposites powders were then investigated. In this experiment, transparent glass and black paper were chosen as the substrates, and commercial powders were selected as the control group. As shown in Fig. 7, even the third level of ridge features (sweat pores) of fingerprints could be

Table 2 The grayscale analysis of fingerprint images on substrates developed by Au@KCC-1 nanocomposites powders

Image	Gray analysis	Grayscale															Gray difference
Glass	Distance	0.0017	0.03	0.0533	0.0733	0.1067	0.135	0.1517	0.1717	0.1933	0.2067	0.2167	0.2433	0.27	0.3167	0.3883	0.4	63.325
	Gray	159.8	101.4	183	107.2	213.5	119.1	147.5	104.4	153.9	130.8	158.9	116.6	204	119.6	204.4	119.3	
Foundation box	Distance	0.0017	0.0217	0.0443	0.08	0.0933	0.1183	0.1467	0.1633	0.1933	0.2133	0.235	0.2483	0.28	0.295	0.3133	0.3317	55.802
	Gray	172.95	120.34	177	121.4	168.85	127.23	202.87	121.16	187.8	122.38	165.66	120.63	175.35	113.36	175.86	133.42	

observed when Au@KCC-1 nanocomposites powders were used as the detecting reagent. However, this delicate information cannot be obtained by commercial powders. Besides, both papillary ridges and furrows were detected by commercial powders, making the ridge details of fingerprints look obscure. In comparison, clear ridges and sharp edges without no background staining were obtained by Au@KCC-1 nanocomposites powders. These results showed that Au@KCC-1 nanocomposites powders have higher sensitivity and selectivity.

As the main basis of individual identification, the ability to reflect the detailed features of latent fingerprints were used to evaluate fingerprint powders. In identity verification, the overall pattern of papillary ridges is the first level of ridge features. Characteristic details, including whorl and termination and so on, are classified to the second level of ridge features, while more detailed features such as sweat pores are the third level of ridge features. The second level of ridge features or higher-level ridge features are more important. In experiments, high-quality fingerprint images obtained from smooth substrates (glass) using Au@KCC-1 nanocomposites powders enabled clear visualization of the features of fingerprints like the island, core, termination, bifurcation, and even sweat pores (Fig. 8). These results strongly proved the high resolution and high detecting quality of Au@KCC-1 nanocomposites powders. Moreover, the visualization results of freshly prepared Au@KCC-1 nanocomposites powders and the powders stored under dry conditions for 6 months were compared to verify the stability of powders, and the results were shown in Fig. 9. Au@KCC-1 nanocomposites powders, as a new kind of fingerprint powders, displayed excellent stability with proper storage methods.

4 Conclusions

In summary, a novel Au@KCC-1 fingerprint powders with significantly increased accessibility of active sites were successfully synthesized. The aminopropyl functionalization of KCC-1 provided robust anchors for the growth of Au NPs, and Au NPs with an average diameter of about 3 nm were well-dispersed on the fibers of the KCC-1 microspheres without aggregation. The obtained Au@KCC-1 nanocomposites powders were able to enhance latent fingerprints with high sensitivity and selectivity by exhibiting strong contrasts, clear ridge details, and distinguishable sweat pores of fingerprints. More importantly, Au@KCC-1 nanocomposites powders were environmentally friendly, sustainable, and biocompatible. Considering these merits, we envision that Au@KCC-1 nanocomposites powders could be an effective alternative to conventional powdering reagents in the future.

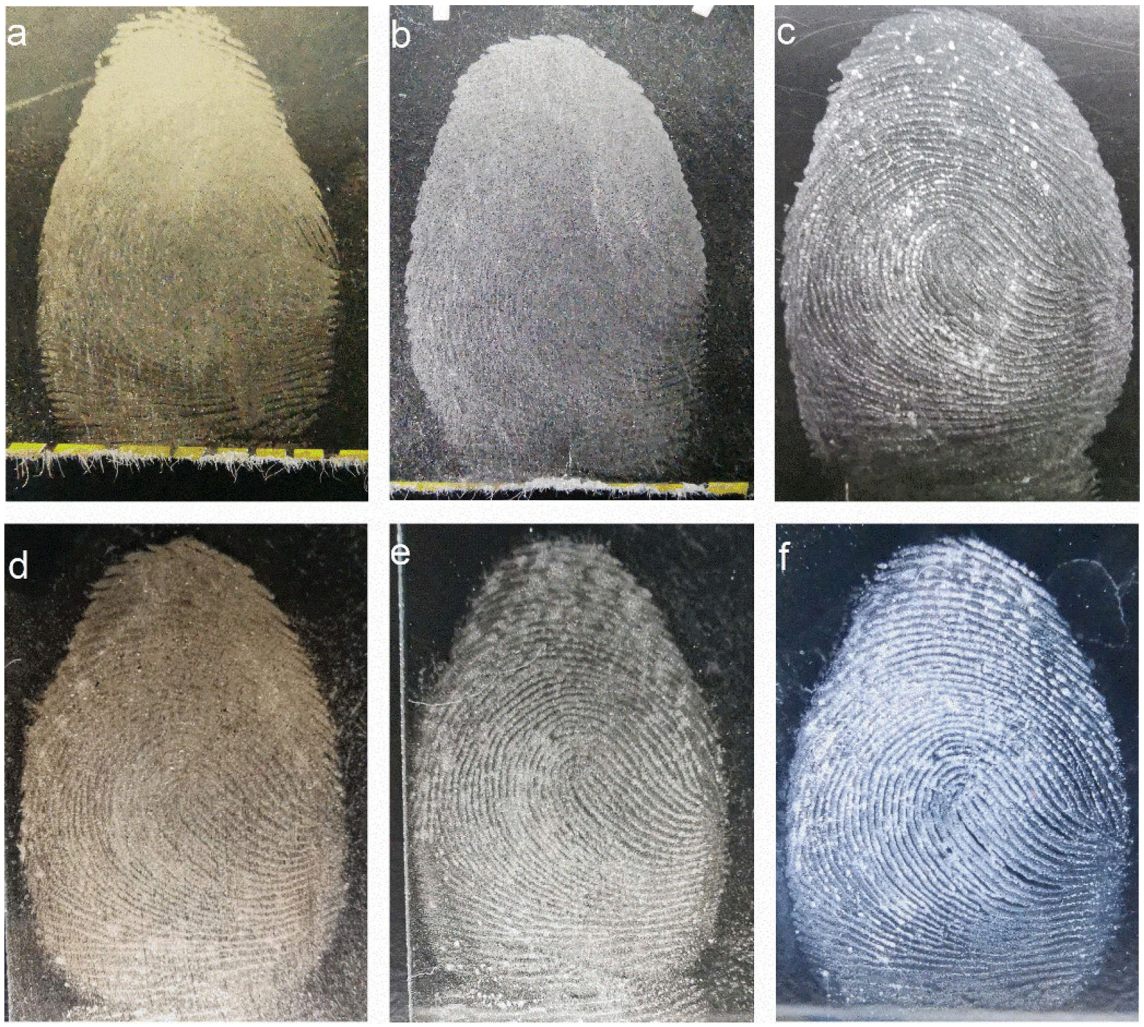

Fig. 7 Development of latent fingerprints on various substrates, using different types of powders: **a–c** black paper, in brightfield; **d–f** glass, in bright field; Left, middle and right rows contain fingerprints powders for gold powders, silver powders, and Au@KCC-1 nanocomposites powders, respectively. Images were taken under visible light, and a VSC6000 document imaging workstation was used to take pictures

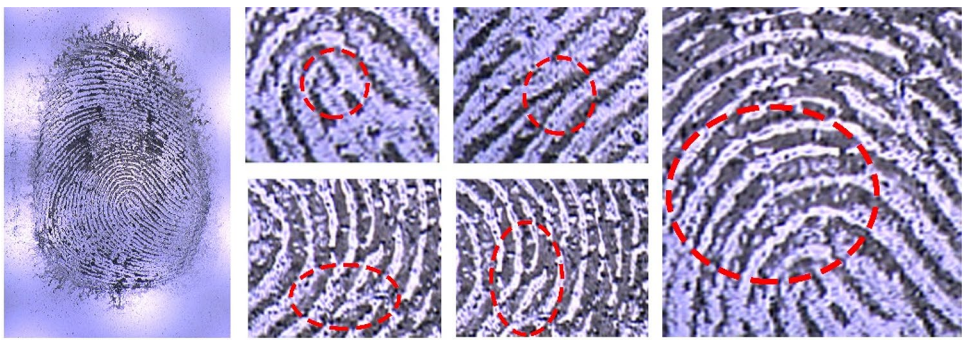

Fig. 8 Specific details of fingerprint images using Au@KCC-1 nanocomposites powders on a glass substrate after 6 months of storage. Images were taken under coaxial light, and a VSC6000 document imaging workstation was used to take pictures

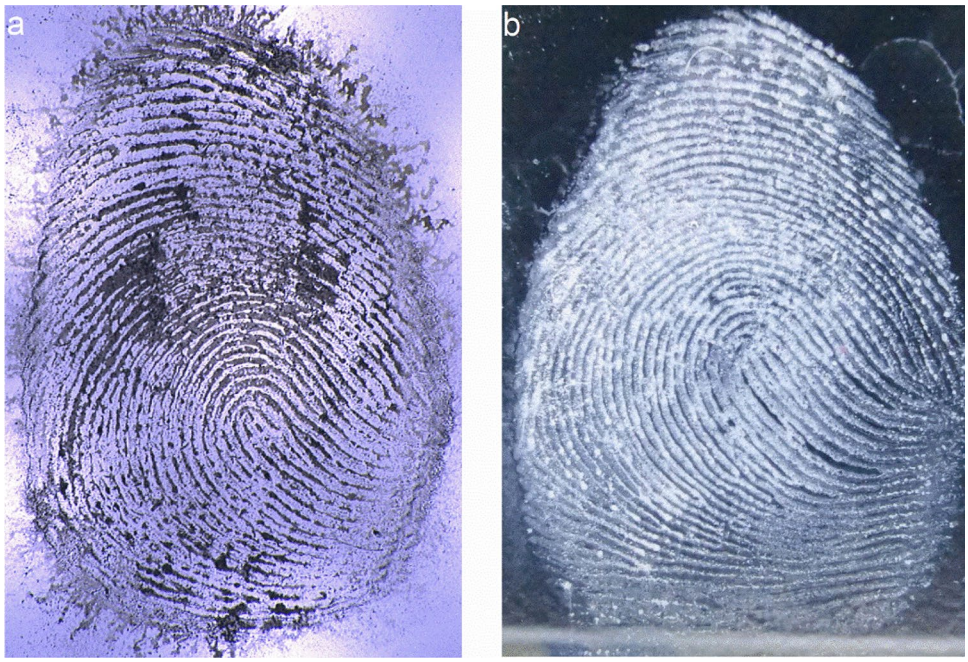

Fig. 9 Stability study of as-prepared Au@KCC-1 nanocomposites powders on glass by using **a** Au@KCC-1 nanocomposites powders stored after 6 months and **b** freshly Au@KCC-1 nanocomposites powders

Acknowledgements This work was supported by the National Natural Science Foundation of China (Grant No. 51501042) and Educational Committee Foundation of Gansu (Grant. No. 2019 A-092).

References

1. K. Li, W.W. Qin, F. Li, X.C. Zhao, B.W. Jiang, K. Wang, S.H. Deng, C.H. Fan, D. Li, Angew. Chem. Int. Ed. **52**, 11542 (2013)
2. J. Wang, T. Wei, X.Y. Li, B.H. Zhang, J.X. Wang, C. Huang, Q. Yuan, Angew. Chem. Int. Ed. **53**, 1709 (2014)
3. J. Wang, Q.Q. Ma, H.Y. Liu, Y.Q. Wang, H.J. Shen, X.X. Hu, C. Ma, Q. Yuan, W.H. Tan, Anal. Chem. **89**, 12764 (2017)
4. P. Wu, C.Y. Xu, X.D. Hou, J.J. Xu, H.Y. Chen, Chem. Sci. **6**, 4445 (2015)
5. X. Ran, Z.Z. Wang, Z.J. Zhang, F. Pu, J.S. Ren, X.G. Qu, Chem. Commun. **52**, 557 (2016)
6. B. Su, Anal. Bioanal. Chem. **408**, 2781 (2016)
7. M. Wang, M. Li, A.Y. Yu, Y. Zhu, M.Y. Yang, C.B. Mao, Adv. Funct. Mater. **27**, 1606243 (2017)
8. X.B. Jia, L.L. Li, J.J. Yu, X.J. Gao, X.J. Yang, Z.M. Lu, X.H. Zhang, H. Liu, Spectrochim. Acta. Part. A. **203**, 214 (2018)
9. Z.H. Li, Q. Wang, Y.Q. Wang, Q.Q. Ma, J. Wang, Z.H. Li, Y.X. Li, X.B. Lv, W. Wei, L. Chen, Q. Yuan, Nano. Res. **11**, 6167 (2018)
10. D. Peng, X. Liu, M.J. Huang, D. Wang, R.L. Liu, Dalton. Trans. **47**, 5823 (2018)
11. L. Yan, Y.L. Yu, Z.N. Xia, Sci. China. Chem. 61, (2018).
12. Z.Q. Deng, C. Liu, Y.Z. Jin, J.L. Pu, B. Wang, J.C. Chen, Analyst 144, (2019).
13. F. Gao, C.F. Lv, J.X. Han, X.Y. Li, Q. Wang, J. Zhang, C. Chen, Q. Li, X.F. Sun, J.C. Zheng, L. Bao, X. Li, J. Phys. Chem. C. **115**, 21574 (2011)
14. S.N. Qu, X.Y. Wang, Q.P. Lu, X.Y. Liu, L.J. Wang, Angew. Chem. Int. Ed. **51**, 12215 (2012)
15. D. Fernandes, M.J. Krysmann, A. Kelarakis, Chem. Commun. **51**, 4902 (2015)
16. S.-J. Ryu, H.-S. Jung, J.-K. Lee, Bull. Korean. Chem. Soc. **36**, 2561 (2015)
17. M. Wang, M. Li, A.Y. Yu, J. Wu, C.B. Mao, ACS. Appl. Mater Interfaces **7**, 28110 (2015)
18. G. Saunders, in *74th Annual Edueational Conference*, Pensaeola, USA, 1989.
19. E. Stauffer, A. Becue, K. V. Singh, K. R. Thampi, C. Champod, P. Margot, Forensic. Sci. Int. 168, (2007).
20. M.J. Choi, A.M. McDonagh, P.J. Maynard, R. Wuhrer, C. Lennard, C. Roux, J. Forensic. Identif. 56, (2006).
21. I. Hussain, S.Z. Hussain, R. Habibur, A. Ihsan, A. Rehman, Z.M. Khalid, M. Brust, A.I. Cooper, Nanoscale 2, (2010).
22. J.J. Zhao, K. Zhang, Y.X. Li, J. Ji, B.H. Liu, ACS. Appl. Mater Interfaces **8**, 14389 (2016)
23. C.J. Yuan, M. Li, M. Wang, L.M. Zhang, Dyes. Pigm. **153**, 18 (2018)
24. Z.L. Wang, X. Jiang, W.B. Liu, G.L. Lu, X.Y. Huang, Sci. China. Chem. **62**, 889 (2019)
25. Y.-Y. Zhou, Y.-M. Du, X.-J. Bian, J. Yan, Chin. J. Anal. Chem. **47**, 998 (2019)
26. D. Fernandes, M.J. Krysmann, A. Kelarakis, Chem. Commun. **52**, 8294 (2016)
27. Y.-J. Kim, H.-S. Jung, J. Lim, S.-J. Ryu, J.-K. Lee, Langmuir **32**, 8077 (2016)
28. W. Huang, X.J. Li, H.F. Wang, X.J. Xu, H. Liu, G.Q. Wang, Anal. Lett. **48**, 1524 (2015)
29. M.Q. Zhang, Y.Y. Ou, X. Du, X.Y. Li, H.W. Huang, Y.Q. Wen, X.J. Zhang, J. Porous. Mater. **24**, 13 (2016)
30. N. Bayal, B. Singh, R. Singh, V. Polshettiwar, Sci. Rep. **6**, 24888 (2016)
31. M.Y. Ouyang, Y. Wang, J. Zhang, Y.J. Zhao, S.P. Wang, X.B. Ma, RSC. Adv. **6**, 12788 (2016)
32. Z.S. Qureshi, P.B. Sarawade, I. Hussain, H. Zhu, H. Al-Johani, D.H. Anjum, M.N. Hedhili, N. Maity, V. D'Elia, J.-M. Basset, ChemCatChem **8**, 1671 (2016)
33. B. Singh, V. Polshettiwar, J. Mater. Chem. A. **4**, 7005 (2016)
34. R. Singh, R. Bapat, L. Qin, H. Feng, V. Polshettiwar, ACS. Catal. **6**, 2770 (2016)

35. Z.P. Dong, X.D. Le, X.L. Li, W. Zhang, C.X. Dong, J.T. Ma, Appl. Catal. B. **158–159**, 129 (2014)
36. E. Febriyanti, V. Suendo, R.R. Mukti, A. Prasetyo, A.F. Arifin, M.A. Akbar, S. Triwahyono, I.N. Marsih, Ismunandar, Langmuir **32**, 5802 (2016)
37. T.J. Siang, A.A. Jalil, M.Y.S. Hamid, A.A. Abdulrasheed, T.A.T. Abdullah, D.V.N. Vo, Fuel **278**, 118360 (2020)
38. A. Maity, A. Das, D. Sen, S. Mazumder, V. Polshettiwar, Langmuir **33**, 13774 (2017)
39. X.D. Le, Z.P. Dong, W. Zhang, X.L. Li, J.T. Ma, J. Mol. Catal. A Chem. **395**, 58 (2014)
40. E. Hutter, J.H. Fendler, Adv. Mater. **16**, 1685 (2004)
41. M. Dhiman, B. Chalke, V. Polshettiwar, J. Mater. Chem. A. **5**, 1935 (2017)
42. W. Byoun, S. Jung, N.M. Tran, H. Yoo, ChemistryOpen **7**, 349 (2018)
43. R. Singh, R. Belgamwar, M. Dhiman, V. Polshettiwar, J. Mater. Chem. B. **6**, 1600 (2018)
44. H.L. Yang, S.W. Li, X.Y. Zhang, X.Y. Wang, J.T. Ma, J. Mater. Chem. A. **2**, 12060 (2014)
45. S.M. Sadeghzadeh, Green. Chem. **17**, 3059 (2015)
46. S.M. Sadeghzadeh, J. Mol. Catal. A Chem. **423**, 216 (2016)
47. A. Fihri, M. Bouhrara, U. Patil, D. Cha, Y. Saih, V. Polshettiwar, ACS. Catal. **2**, 1425 (2012)
48. Q.H. Wei, M.Q. Zhang, B. Ogorevc, X.J. Zhang, Analyst **141**, 6172 (2016)
49. Y.Q. Wang, J. Wang, Q.Q. Ma, Z.H. Li, Q. Yuan, Nano. Res. **11**, 5499 (2018)
50. Y.Y. He, L.R. Xu, Y. Zhu, Q.H. Wei, M.Q. Zhang, B. Su, Angew. Chem. Int. Ed. **53**, 12609 (2014)
51. G.S. Sodhi, J. Kaur, Forensic. Sci. Int. **120**, 172 (2001)
52. D. Peng, X. Wu, X. Liu, M.J. Huang, D. Wang, R.L. Liu, ACS. Appl. Mater. Interfaces. **10**, 32859 (2018)
53. J. Chen, J.-S. Wei, P. Zhang, X.-Q. Niu, W. Zhao, Z.-Y. Zhu, H. Ding, H.-M. Xiong, ACS. Appl. Mater. Interfaces. 9 (2017).
54. F. Gao, J.X. Han, J. Zhang, Q. Li, X.F. Sun, J.C. Zheng, L.R. Bao, X. Li, Z.L. Liu, Nanotechnology 22, (2011).